ISSN (Print) 1226-1750
ISSN (Online) 2233-6656
Journal of Magnetics 30(4), 606-614 (2025) https://doi.org/10.4283/JMAG.2025.30.4.606

Design and Pressure Drop Performance of Mixed Flow Channel Magnetorheological Valve

Yangyang Guo[1], Minjian Zhu[1], Zuzhi Tian[1]*, Xiangfan Wu[2], and Haopeng Li[1]

[1]*School of Mechanical and Electrical Engineering, China University of Mining and Technology, Xuzhou, 221116, China*
[2]*School of Mechanical and Electrical Engineering, Xuzhou University of Technology, 221018, China*

(Received 12 June 2025, Received in final form 14 October 2025, Accepted 15 October 2025)

The present study proposes a novel design of a dual coil magnetorheological valve, incorporating disc and circular flow channels, to address the issues associated with low channel utilisation and limited adjustable range of pressure drop in the conventional magnetorheological valve. Firstly, the magnetic circuit design and calculation of the magnetorheological valve are conducted based on the dual-coil structure. Subsequently, electromagnetic simulation analysis is performed using COMSOL to investigate the distribution law of magnetic induction intensity in the working area of the magnetorheological valve under varying currents and runner gaps. Secondly, a mathematical model of the pressure drop of the dual coil magnetorheological valve with mixed flow channel is developed, and the effects of parameters such as flow gap, operating flow rate and current on the pressure drop characteristics are investigated. Results demonstrate that the adjustable pressure drop of the magnetorheological valve ranges from 0.421 to 10.391 MPa with an excitation current of 2.5 A and a flow gap of 1.5 mm, which effectively broadens the adjustable range of the pressure drop and the applicable working conditions.

Keywords : magnetorheological valve, magnetic circuit design, electromagnetic field analysis, pressure drop

1. Introduction

Magnetorheological (MR) fluid is a novel type of intelligent fluid, which is unique in its rheological effect, in the applied magnetic field excitation MR fluid can be solidified by the Newtonian fluid state converted to a non-Newtonian fluid state, so that have a certain yield strength, and can be withdrawn from the applied magnetic field from the solid state back to the liquid state, the conversion of this rapid and controllable [1-3]. MR fluid's unique properties make it in the mechanical, hydraulic and control fields have great potential, caused a wide range of domestic and foreign scholars on the attention. The use of MR fluid as a working medium has been applied to many industrial fields, including governor, clutches, brakes, shock absorbers, hydraulic valves and seals and other equipment [4-7].

At present, with the development of hydraulic technology intensification and intelligence, the traditional hydraulic valve due to the complex structure, multi-component action control difficulties and manufacturing precision requirements are too high, it has been difficult to meet the demand for mechanical-fluid-control coupling. Some scholars have begun to turn to the structure of a simpler, no action parts and fluid pressure intelligently controllable MR valves to carry out research, and has made good progress in the study [8, 9].

MR valve is a new type of intelligent valve that utilizes MR fluid as the working medium, and adjusts the overall pressure drop of the MR valve by applying a magnetic field that acts on the MR fluid to produce a controllable yield strength [10]. Various MR valve configurations have been proposed in order to provide the MR valve with a higher adjustable range of pressure drop.

Zhu *et al.* [10] investigated the effect of built-in and external coils on the performance of MR valves, and the results showed that the external coil has a higher pressure drop under the same operating conditions. Imaduddin *et al.* [11] proposed a compact MR valve structure formed by annular and radial gaps, and the results showed that multiple gaps can effectively improve its pressure drop performance. Yang *et al.* [12]

*Corresponding author: +Tel: 86-13914876762
Fax: +86-0516-83590777, e-mail: zuzhitian2022@163.com

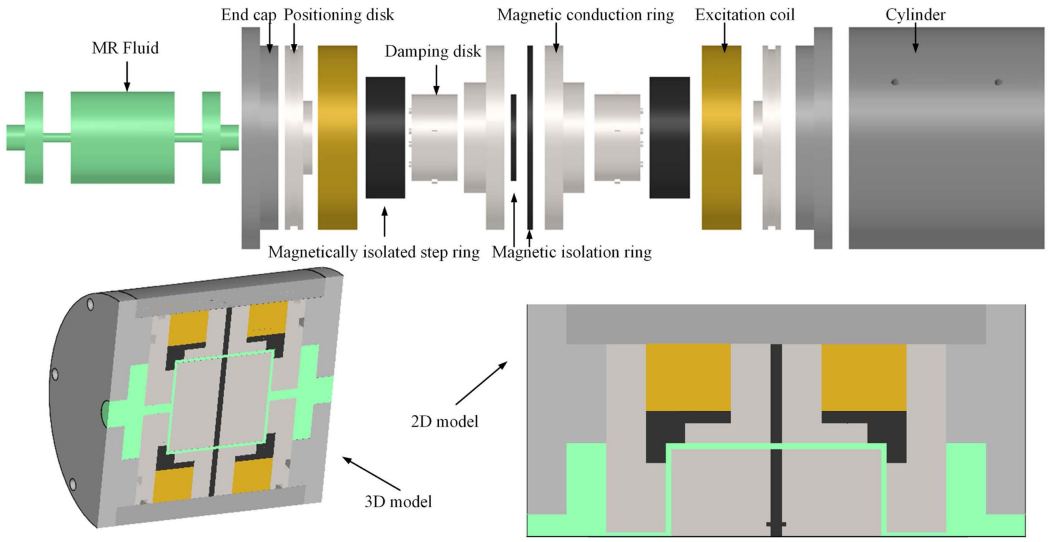

Fig. 1. (Color online) Structure of the dual coil MR valve.

and Sun *et al.* [13] proposed the hybrid magnet-source MR valve structure, which can improve the MR valve voltage drop and can be used in the absence of current through the combination of permanent magnets and excitation coils as compared to the single-excitation structure. Yang *et al.* [14] also designed a multi-ring, multi-disk MR valve and experimentally investigated the pressure drop characteristics under different operating conditions. The results show that the pressure drop of the MR valve can reach more than 7 MPa. Hu *et al.* [15] designed and tested a dual-coil MR valve with an outer ring resistance gap, which significantly improved the efficiency of the dual-coil MR valve. Kubik *et al.* [16] proposed a three-coil MR valve structure, and the results showed that the adjustable range of pressure drop of the three-coil MR valve is 8, which is better than the conventional structure.

In order to improve the pressure drop performance of MR valves, the above scholars mainly use multiple coils with multiple channels, but the multi-coil structure exists mutual interference, which will cause magnetic field loss. In this paper, a dual coil MR valve structure is proposed, in which the dual coils do not interfere with each other and can act individually or together, making full use of the axial and radial working gaps, increasing the magnetic field utilization, and improving the pressure drop performance of the MR valve.

2. Principle of MR Valve

2.1. Structure of MR Valve

The structure of the dual coil MR valve proposed in this paper is shown in Fig. 1. The MR valve mainly consists of end caps, positioning disks, excitation coils, spacer rings, conductive rings, damping disks and MR fluid. When working, the excitation coil is energized to generate a magnetic field, which acts on the MR fluid in the working gap, turning it from liquid to solid, generating magnetotropic yield stress and hindering the MR fluid from passing through, so as to change the pressure difference between the inlet and outlet of the magneto-rheological valve. By changing the current size of the excitation coil, the magnetotropic yield stress of the MR fluid will be changed accordingly, so as to realize the regulation of the pressure difference between the inlet and outlet of the MR valve.

Under the action of the applied magnetic field, the MR fluid solidifies and presents a certain shear yield strength, thus generating a pressure difference, the size of which is related to the size of the applied magnetic field; therefore, the magnetic circuit design is the key to the MR valve design. During the design process, it is necessary to ensure that the magnetic line of force passes through the working area as perpendicularly as possible, so as to improve the utilization rate of the magnetic circuit. Fig. 2 shows the simplified MR valve magnetic circuit structure, and Fig. 3 shows its equivalent magnetic circuit. The key dimensional parameters of the MRvalve are shown in Table 1.

The magnetic circuit of the MR valve consists of a cylinder barrel, a magnetically conductive part and a magnetorheological fluid, as shown in Fig. 2: ① axial portion of the cylinder, ② radial portion of the positioning disk, ③ axial portion of the positioning disk, ④ axial MR

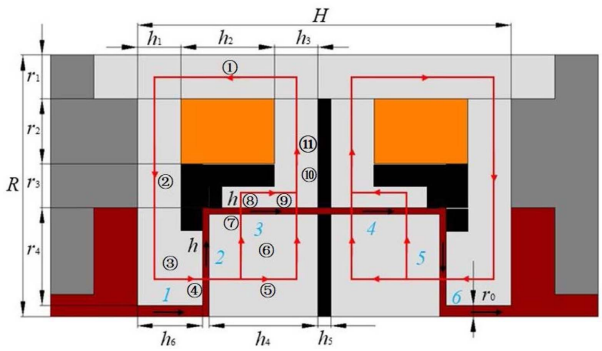

Fig. 2. (Color online) Magnetic circuit of MR valve.

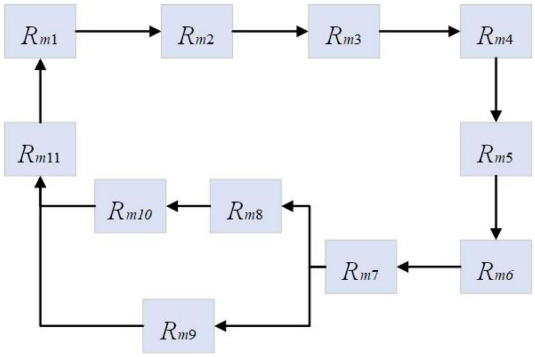

Fig. 3. (Color online) Equivalent magnetic resistance of MR valve.

Table 1. Key parameters of the MR valve.

Parameter	Size/mm	Parameter	Size/mm
H	86	R	60
h_1	10	r_0	2.5
h_2	21.5	r_1	10
h_3	10	r_2	15
h_4	25	r_3	10
h_5	3	r_4	22.5
h_6	15	h	1.5

fluid portion, ⑤ axial portion of the damper disk, ⑥ and ⑦ radial portion of the damping disk, ⑧ radial MR fluid portion, and ⑨, ⑩, and ⑪ radial magnetically conductive ring portion.

According to Ohm's law, the magnetoresistance of the MR valve can be expressed as:

$$R_{mk} = \frac{l_k}{\mu_0 \mu_k A_k} \tag{1}$$

Where, R_{mk} denotes the magnetoresistance of the k_{th} section of the magnetic circuit, l_k denotes the effective length of the k_{th} section of the magnetic circuit, μ_0 denotes the absolute permeability of the air, μ_k denotes the relative permeability of the magnetic-conducting material of the kth section of the magnetic circuit, and A_k denotes the effective cross-sectional area of the k_{th} section of the magnetic circuit.

Therefore, the magnetoresistance of each magnetic circuit is:

$$R_{m1} = \frac{l_1}{\mu_0 \mu_1 A_1} \quad R_{m2} = \frac{l_2}{\mu_0 \mu_2 A_2} \quad R_{m3} = \frac{l_3}{\mu_0 \mu_3 A_3}$$

$$R_{m4} = \frac{l_4}{\mu_0 \mu_4 A_4} \quad R_{m5} = \frac{l_5}{\mu_0 \mu_5 A_5} \quad R_{m6} = \frac{l_6}{\mu_0 \mu_6 A_6}$$

$$R_{m7} = \frac{l_7}{\mu_0 \mu_7 A_7} \quad R_{m8} = \frac{l_8}{\mu_0 \mu_8 A_8} \quad R_{m9} = \frac{l_9}{\mu_0 \mu_9 A_9}$$

$$R_{m10} = \frac{l_{10}}{\mu_0 \mu_{10} A_{10}} \quad R_{m11} = \frac{l_{11}}{\mu_0 \mu_{11} A_{11}} \tag{2}$$

The effective lengths of each magnetic circuit are respectively:

$$l_1 = h_2 + \frac{h_1 + h_3}{2} \quad l_2 = \frac{r_1}{2} + r_2 + r_3 + \frac{r_4}{2} \quad l_3 = h_6 - \frac{h_1}{2} \quad l_4 = h$$

$$l_5 = h_4 - \frac{h_3}{2}$$

$$l_6 = \frac{r_4 - h}{2} \quad l_7 = h \quad l_8 = \frac{r_3}{2} \quad l_9 = \frac{h_4 - h_3}{2} \quad l_{10} = r_3 \quad l_{11} = r_2 \tag{3}$$

The effective cross-sectional areas of each magnetic circuit are respectively:

$$A_1 = \pi \left[R^2 - (R - r_1)^2 \right] \quad A_2 = \pi \left(R - \frac{r_1}{2} \right) h_1$$

$$A_3 = \pi \left[(r_4 + r_0)^2 - r_4^2 \right]$$

$$A_4 = \pi \left[(r_4 - h)^2 - r_0^2 \right] \quad A_5 = \pi \left[(r_4 - h)^2 - r_0^2 \right]$$

$$A_6 = \pi (r_4 - h) h_4$$

$$A_7 = \pi r_4 h_4 \quad A_8 = \pi (r_4 + r_0) \frac{h_4 - h_3}{2}$$

$$A_9 = \pi \left[(R - r_1 - r_2)^2 - (r_4 + r_0)^2 \right]$$

$$A_{10} = \pi (R - r_1 - r_2) h_3 \quad A_{11} = \pi (R - \frac{r_1}{2}) h_3 \tag{4}$$

The magnetic resistance at the parallel connection is:

$$\frac{1}{R_{mb}} = \frac{1}{R_{m8} + R_{m9}} + \frac{1}{R_{m10}} \tag{5}$$

The shunt reluctance can be calculated as:

$$R_{mb} = \frac{(R_{m8} + R_{m9}) R_{m10}}{R_{m8} + R_{m9} + R_{m10}} \tag{6}$$

The total magnetic resistance of the magnetic circuit of the magnetorheological valve is:

$$R_m = \sum_{k=1}^{7} R_{mk} + R_{mb} + R_{m11} \tag{7}$$

According to Kirchhoff's second law, the magnetic circuit flux of the magnetorheological valve is:

$$\Phi = \frac{NI}{R_m} = \frac{NI}{\sum_{k=1}^{7} R_{mk} + R_{mb} + R_{m11}} \tag{8}$$

It is known that the working area of the MR fluid in the flow path of the MR valve is A_4, and according to the nature of the MR fluid itself, it can be determined that the magnetic induction strength of the MR fluid in the working flow path is B_4, and the magnetic flux of the magnetic circuit is equal at all places under the ideal working condition, so the magnetic flux of the magnetic circuit of the MR valve can be expressed as follows:

$$\Phi = B_4 S_4 \tag{9}$$

Then, the number of excitation coil ampere-turns can be obtained as:

$$NI = B_4 S_4 R_m \tag{10}$$

The calculated ampere-turns amount to 683. Given the maximum input current of 2.5 A, the number of coil turns must be greater than 275 to meet this requirement. Accordingly, the number of turns has been rounded up and set to 300.

3. Electromagnetic Field Simulation

Electromagnetic field simulation is an important link in the design of MR valve, and the validity of the structural design can be verified through the results of electromagnetic field simulation. COMSOL is a professional electromagnetic simulation software, and it is easy to operate and convenient for data processing. In this paper, COMSOL software is used to analyze the electromagnetic field simulation of the designed MR valve.

3.1. Preprocessing of the simulation

To comprehensively illustrate the distribution of magnetic induction intensity within the MR valve and the MR fluid, both 2D and 3D simulations were conducted concurrently. Fig. 4 shows the MR valve simulation model, the material is applied to each part and meshed by the software. Fig. 5 shows the *B*-*H* curve of MR fluid.

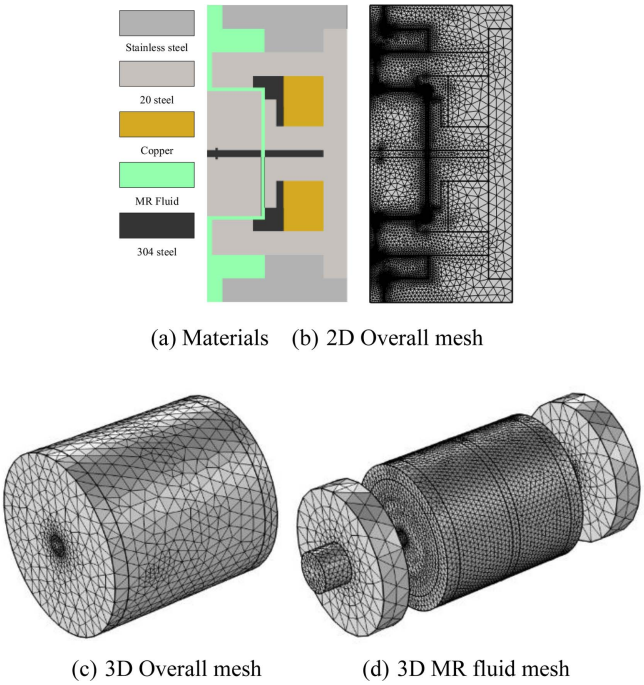

(a) Materials (b) 2D Overall mesh

(c) 3D Overall mesh (d) 3D MR fluid mesh

Fig. 4. (Color online) Material and mesh.

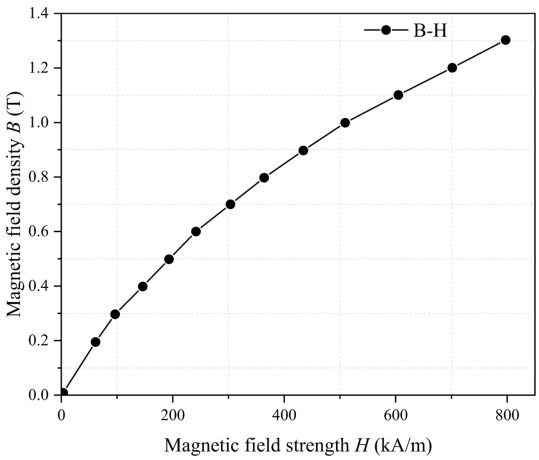

Fig. 5. B-H curve of MR fluid.

3.2. Analysis of simulation results

When 2.5 A excitation current is applied to the coils, with each coil having 300 turns and flow channel gap of 1.5 mm, the distribution of the magnetic induction intensity obtained is shown in Fig. 6.

As can be seen in Fig. 6, the distribution of magnetic lines of force is relatively uniform, basically passing completely through the magnetically conductive parts and perpendicularly through the MR fluid flow channel, with high magnetic field utilization. The magnetic induction intensity in the radial working gap (flow channel 2 and 5) is up to 1.08 T. And the smallest one is at the liquid inlet. The magnetic induction intensity in the axial working gap

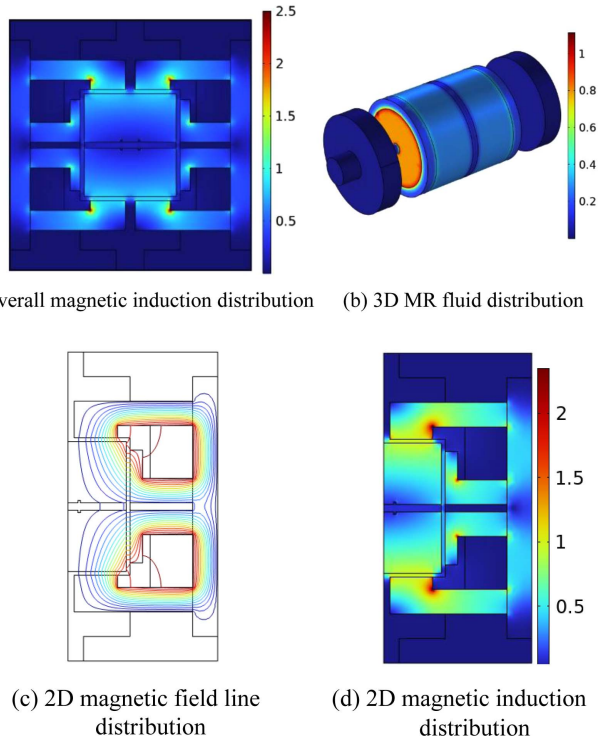

(a) Overall magnetic induction distribution (b) 3D MR fluid distribution

(c) 2D magnetic field line distribution (d) 2D magnetic induction distribution

Fig. 6. (Color online) Magnetic field simulation result.

(flow channel 3 and 4) is up to 0.38 T, and the smallest one is at the spacer ring. Besides, the magnetic field of the double coils does not interfere with each other, which indicates that the spacer ring has played a good effect of magnetic isolation. The distribution of the overall magnetic induction intensity is in line with the design expectation.

3.3. Analysis of different influences

The magnitude of the current and the size of the working gap have significant influences on the magnetic induction intensity distribution of the MR valve. This section will conduct research on the distribution law of magnetic induction intensity under different currents and different flow channel gaps.

3.3.1 Current

The number of turns of the MR valve coil is set to 300, the working gap is set to 1.5 mm, and the excitation current is taken to be in the range of 0.5~3.0 A with an interval of 0.5 A. The distribution curves of the magnetic induction intensity of the flow channel under different excitation currents are shown in Fig. 7.

According to Fig. 7 and Fig. 8, it is evident that the symmetrical structure of MR valve working flow channel 2 and 5 exhibits consistent magnetic induction intensity distributions under identical operating conditions. As the current increases, the magnetic induction intensity rises from 0.33 T to 1.08 T, with increments of 63.5%, 33.1%, 21.0%, 14.7%, and 8.1% in magnitude, respectively. The rate of increase gradually diminishes, indicating that the magnetic induction intensity asymptotically approaches a constant value.

The variation of the magnetic induction curves for flow channel 3 and 4 is depicted in Fig. 8(b). As the current increases from 0.5 A to 2.5 A, the magnetic induction also increases, with the rate of increase progressively decreasing from 68.3% to 15.0%. When the current is further increased from 2.5 A to 3.0 A, the magnetic induction intensity rises from 0.38 T to 0.48 T, corresponding to an increase of 24.6%. This behavior occurs because the MR fluid has not yet reached magnetic saturation within the range of 0.5~3.0 A, allowing the magnetic induction strength to continue increasing significantly with the current.

3.3.2 Working gap

In order to study the magnetic field distribution of the MR valve under different flow channel gaps, the number of turns of the excitation coil is set to be 300, the current is set to be 1.5 A, and the working gaps are in the range of 0.5~2.0 mm at intervals of 0.5 mm to carry out the simulation analysis of the electromagnetic field.

Fig. 9 shows the distribution curve of the magnetic induction intensity of the working flow channel of the MR valve with different working gaps. As can be seen in Fig. 9, the magnetic induction intensity increases as the working gap decreases. The magnetic induction intensity at flow channel 3 and 4 increased by 24.5%, 29.7% and 54.2% when the gap was reduced from 2.0 mm to 0.5 mm, respectively. At flow channel 2 and 5, it increased by 20.5%, 27.0% and 40.0%, respectively. The working gap that is too small may result in difficulties in machining and assembly, while the working gap that is too large may cause insufficient magnetic induction. Consequently, the design of an MR valve should take into account various factors to determine the appropriate gap size. To ensure both a sufficiently large adjustable pressure drop range and ease of manufacturing and assembly for the MR valve, this study adopts a gap size of 1.5 mm.

3.3.3 Energization of the coil

To investigate the magnetic field distribution of the MR valve under various coil energization conditions, the excitation coil was configured with 300 turns, the current was set to 2.5 A, and the flow channel gap was maintained at 1.5 mm. Fig. 10 shows the distribution of magnetic induction intensity for all flow channels (the

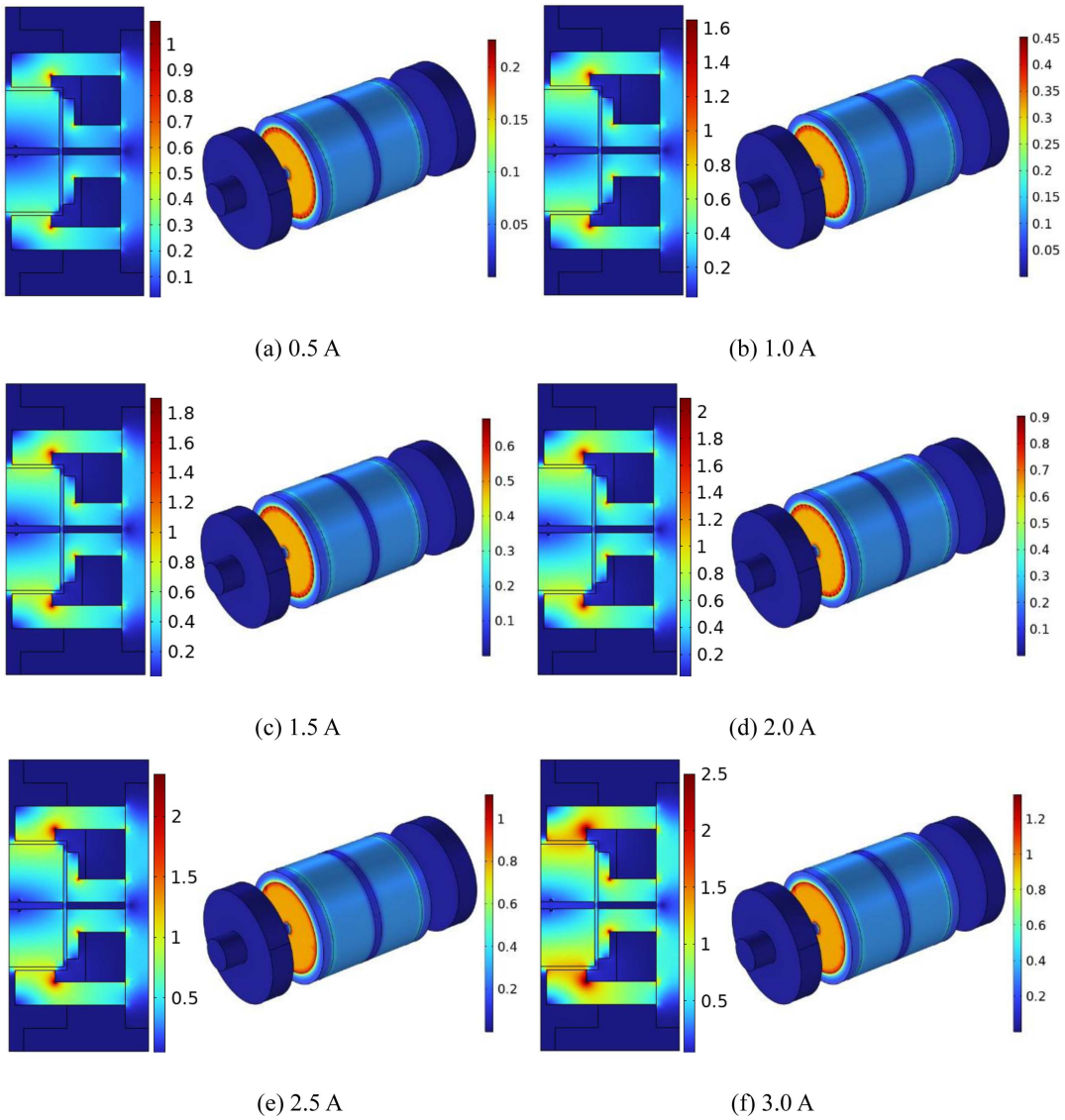

Fig. 7. (Color online) Magnetic induction of MR fluid under different currents.

flow channels shown in Fig. 2, from flow channel 1 to flow channel 6).

As illustrated in Fig. 10, the distribution patterns of magnetic induction intensity are consistent when coil 1 and coil 2 are energized individually. When both coils are energized simultaneously, the resulting magnetic induction intensity distribution represents the superposition of the two individual fields, indicating that the magnetic isolation ring effectively prevents magnetic interference between the coils and verifies the effectiveness of the dual coil structure.

4. Analysis of Pressure Drop

In this paper, the MR fluid is selected as MRF-J25T, and its shear yield stress curve are shown in Fig. 11. Its shear yield stress expression can be obtained by fitting as:

$$\tau_y = -126.7535B^3 + 206.0692B^2 - 8.0352B + 1.4392 \quad (11)$$

4.1. Mathematical model of pressure drop

The total pressure drop of the MR valve consists of a viscous pressure drop and a yield pressure drop, which in turn consist of a radial pressure drop and an axial pressure drop, respectively.

The axial pressure drop equation can be expressed as:

$$\Delta p_z = \frac{12\eta q l}{b_k h^3} + \frac{3 l_k \tau_{ky}}{h} \quad (12)$$

Where, η is the zero-field viscosity of the MR fluid

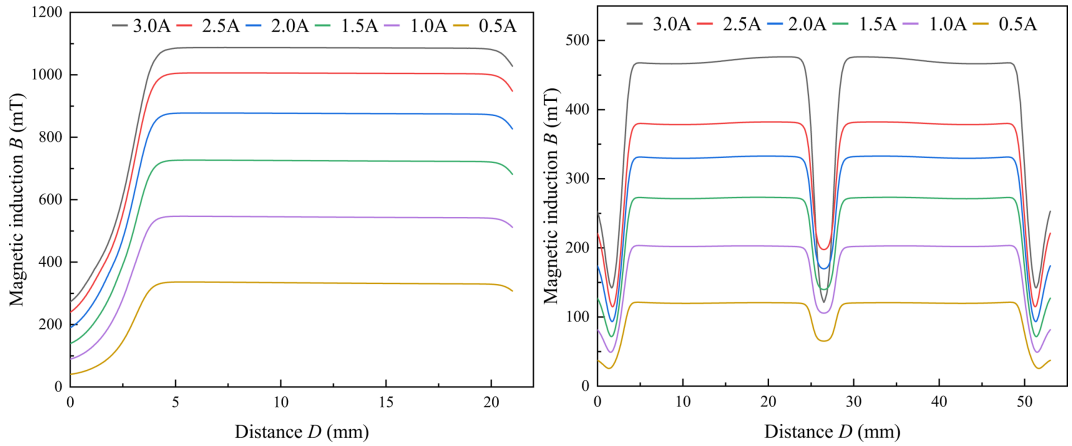

(a) flow channel 2 and 5 (b) flow channel 3 and 4

Fig. 8. (Color online) Magnetic induction of the flow channel under different currents.

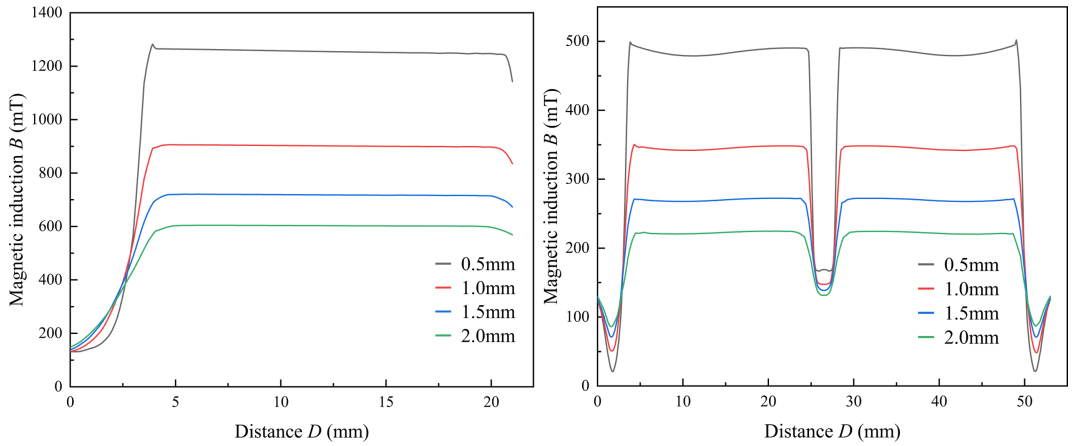

(a) flow channel 2 and 5 (b) flow channel 3 and 4

Fig. 9. (Color online) Magnetic induction of the flow channel under different gaps.

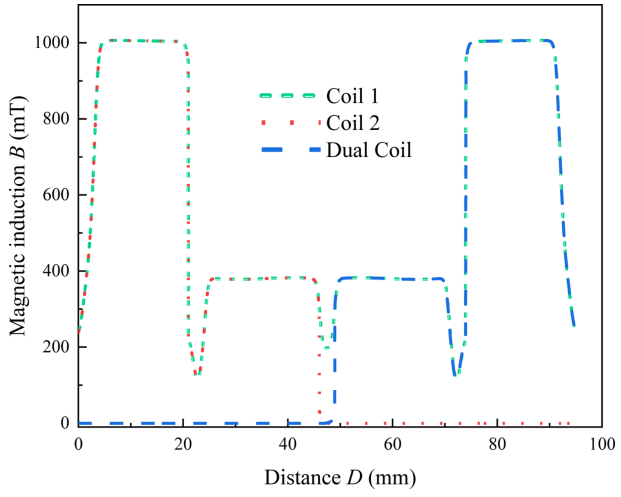

Fig. 10. (Color online) Magnetic induction distribution under different coil energizations.

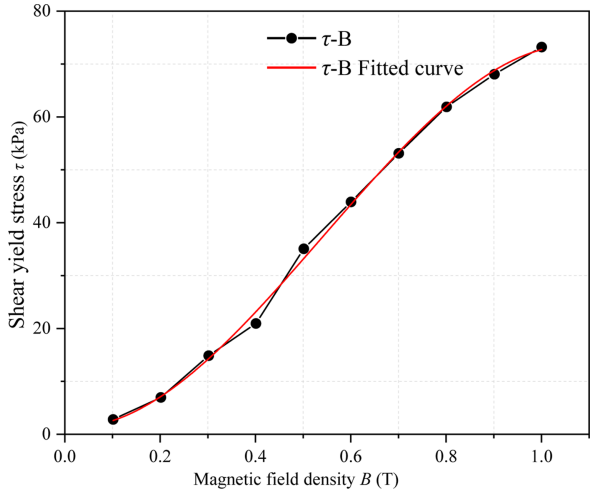

Fig. 11. (Color online) Shear yield stress curve of MRF-J25T.

(0.8Pa·s), l_k is the length of the fluid flow channel, b_k is the MR fluid width of the k_{th} flow channel, h is the working gap, and τ_{ky} is the MR fluid shear in the k_{th} flow channel.

The radial pressure drop equation can be expressed as:

$$\Delta p_j = \frac{6\eta q}{\pi h^3}\ln\frac{R}{r} + \frac{3l\tau_{ky}}{h} \tag{13}$$

Where R is the beginning of the liquid flow path and r is the end of the liquid flow path.

After the excitation coil is energized, there are no magnetic lines of force passing through the flow channel 1 and 6, and only viscous pressure drop is generated, and there are magnetic lines of force passing through the liquid flow channel 2~5, and both viscous pressure drop and yield pressure drop are generated.

The total pressure drop produced by the MR valve can be expressed as:

$$\Delta p_f = \sum_{k=1}^{6}\Delta p_k = \Delta p_1 + \Delta p_2 + \Delta p_3 + \Delta p_4 + \Delta p_5 + \Delta p_6$$
$$= \frac{12\eta q h_6}{\pi r_0 h^3} + \frac{12\eta q}{\pi h^3}\ln\frac{r_4 + r_0}{r_0} + \frac{24\eta q h_4}{b_3 h^3} + \frac{3(r_4 + r_0)(\tau_{2y} + \tau_{5y})}{h}$$
$$+ \frac{3h_4(\tau_{3y} + \tau_{4y})}{h} \tag{14}$$

4.2. Pressure drop performance

The working condition of the MR valve is set to 300 coil turns, the flow rate is 6 L/min, the flow gap is 1.5 mm, and the excitation currents in the range of 0~2.5A are applied to the single and double coils, respectively, at intervals of 0.5A. Then the pressure drop performance curves of the MR valve are obtained, as shown in Fig. 12. The curves of the effect of current magnitude and flow rate magnitude on the pressure drop performance are shown in Fig. 12(b) and (c) for single coil and dual coil condition.

The pressure drop of the MR valve increases with the increase of current and with the increase of flow rate, and the magnitude of the increase all decreases gradually and stabilizes. In the flow rate of 6 L/min, coil turns 300, the maximum pressure drop of single coil can be up to 5.2 MPa, the maximum pressure drop of double coil can be up to 9.556 MPa. In the flow rate of 12 L/min, coil turns 300, and the current of 2.5.A conditions, the maximum pressure drop of the single coil is 6.041 MPa, the maximum pressure drop of the double coil is 10.391 MPa. When the current is 0, the pressure drop of the MR valve is only generated by the viscous pressure drop, the pressure drop is 0.421 MPa when the flow rate is 3 L/min, and the pressure drop is 1.685 MPa when the flow

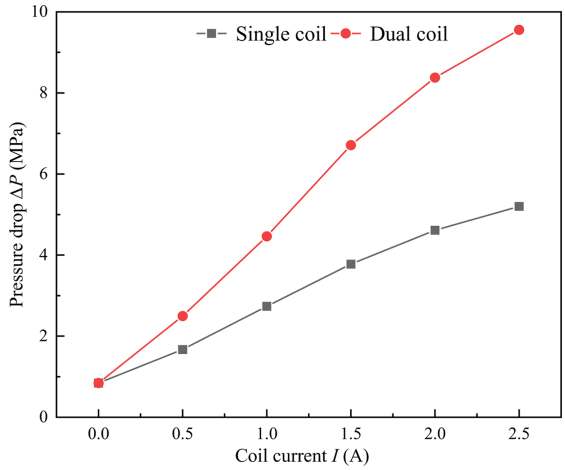

(a) Pressure drop

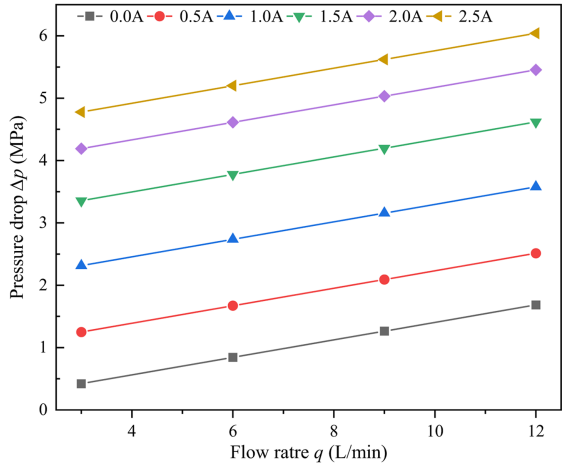

(b) Single coil

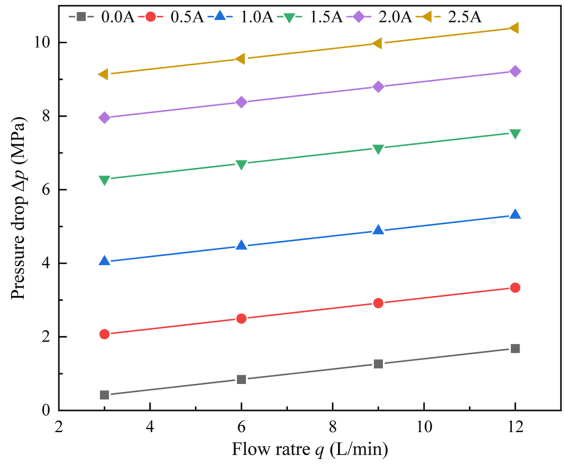

(c) Dual coil

Fig. 12. (Color online) Pressure drop performance of MR valve.

rate is 12 L/min. The MR valve designed in this paper has a good performance, and the dual coils act independently of each other without interfering with each other, and the pressure drop is adjustable in the range of 0.421-10.391 MPa.

5. Conclusion

In this paper, the MR valve with dual coil structure is proposed. And structural design, electromagnetic simulation analysis and pressure drop performance study are carried out, and the following points are concluded.

(1) Based on the structural characteristics of the dual coil MR valve, the magnetic circuit design and magneto-resistance calculation are carried out. The electromagnetic simulation analysis of the MR valve was carried out, and the distribution law of magnetic induction intensity in the working area was investigated by changing the size of the excitation current and the size of the flow channel gap. Results verify the validity of the MR valve structure, and the magnetic fields of the double coils are independent of each other and do not interfere with each other. The maximum magnetic induction strengths for the radial and axial flow channels reach 1.08 T and 0.48 T, respectively, satisfying the operational requirements.

(2) Based on the mathematical model of MR valve, the pressure drop performance analysis was carried out, and the MR valve proposed has a large adjustable range of pressure drop (0.421~10.391 MPa), which has a good scope of application.

The results of the paper can provide some guidance for the design and application of MR valves.

Acknowledgment

This research was supported by the National Natural Science Foundation of China (52375069, 52305078), and the Basic Science (Natural Science) Research Project of the Jiangsu Higher Education Institutions Project Funding (22KJA460013).

References

[1] Z. Z. Tian, X. F. Wu, X. M. Xiao, and F. Chen, J. Magn. **24**, 634 (2019).
[2] X. F. Wu, C. H. Huang, and Z. Z. Tian, Smart Mater. Struct. **28**, 055021 (2019).
[3] R. C. Bell and N. M. Wereley, Int. J. Smart Nano. Mater. **13**, 626 (2022).
[4] Y. Y. Guo, Z. Z. Tian, X. F. Wu, W. Liu, and H. P. Li, J. Magn. **29**, 217 (2024).
[5] X. Y. Zhu, X. L. Yang, and Z. Q. Cao, Phys. Scripta. **99**, 105024 (2024).
[6] M. K. Thakur and C. Sarkar, Defence. Sci. J. **70**, 575 (2020).
[7] J. Wang, X. N. Zhang, and Y. F. Liu, Mech. Syst. Signal PR. **208**, 111040 (2023).
[8] S. L. Ntella, A. Thabuis, and B. Tiwari, IEEE Robot. Autom. Let. **8**, 1487 (2023).
[9] G. L. Hu, F, Zhou, X. Yang, L. F. Yu, and G. Li, J. Magn. Magn. Mater. **589**, 171589 (2024).
[10] X. C. Zhu, X. J. Jing, and L. Chen, J. Intel. Mat. Syst. Str. **24**, 108 (2013).
[11] F. Imaduddin, S. A. Mazlan, H. Zamzuri, and I. I. M. Yazid, J. Intel. Mat. Syst. Str. **26**, 1038 (2015).
[12] X. L. Yang, Y. Li, S. Y. Zhou, and J. H. Zhu, J. Magn. **28**, 124 (2023).
[13] A. X. Sun, F. W. Xie, S. X. Yu, X. W. Shi, J. J. Jie, Y. H. Gao, and K. W. He, Smart Mater. Struct. **32**, 045011 (2023).
[14] X. L. Yang, Z. Q. Cao, G. Liu, and G. J. H. Xie, Smart Mater. Struct. **32**, 025015 (2023).
[15] G. L. Hu, M. Long, M. Huang, and W. H. Li, Advan. Mechan. Engin. **6**, 403410 (2014).
[16] M. Kubik, O. Machacek, Z. Strecker, and J. Roupec, Smart Mater. Struct. **26**, 047002 (2017).